U-Pb zircon geochronology of intrusive rocks from an exotic block in the Late Cretaceous - Paleocene Tarakli Flysch (northern Turkey): constraints on the tectonics of the Intrapontide suture zone

Maria Di Rosa[a,b], Federico Farina[c], Michele Marroni[a,d], Luca Pandolfi[a,d], M. Cemal Göncüoğlu[e], Alessandro Ellero[d], Giuseppe Ottria[d]

a Dipartimento di Scienze della Terra, Università di Pisa, Italy

b Dipartimento di Scienze della Terra, Università di Firenze, Italy

c Department of Earth Sciences, University of Geneva, Switzerland

d Istituto di Geoscienze e Georisorse, CNR, Pisa, Italy

e Department of Geological Engineering, Middle East Technical University, Ankara, Turkey.

==========

* CORRESPONDING AUTHOR:

DR. MARIA DI ROSA,

DIPARTIMENTO DI SCIENZE DELLA TERRA,

UNIVERSITÀ DI PISA, VIA S. MARIA, 53

56126 PISA, ITALY.

E-MAIL: maria.dirosa@unifi.it

ABSTRACT

In the Boyalı area (northern Anatolia), a thick succession of the Early Maastrichtian - Middle Paleocene Taraklı Flysch crops out. The Taraklı Flysch represents a foredeep sediment deposited during the final stage of collision between the Sakarya and Istanbul-Zonguldak continental margins, that developed as a consequence of the closure of the Intrapontide oceanic basin.

The top of the Taraklı Flysch is characterized by a level of slide-block in shaly-matrix lithofacies that can be considered as the result of several fast catastrophic events predating the closure of the basin and its deformation. This level consists of slide-blocks surrounded by monomict pebbly-mudstones and pebbly-sandstones. Among the slide-blocks, the biggest one consists of quartz-monzonites and leucocratic granodiorites of Late Permian age (260.8 ± 2.2 Ma) dated by zircon LA-ICP-MS method. By comparison with the regional data, the source area of these granitoids can be identified in the Istanbul-Zonguldak terrane. This evidence suggests a new picture for the paleogeographic setting of the ultimate stage of the continental collision between the Istanbul-Zonguldak and the Sakarya continental margins. In this scenario the coarse-grained deposits of the Taraklı Flysch are supplied by an orogenic wedge, consisting of oceanic units topped by the Istanbul-Zonguldak terrane. This orogenic wedge represented the north side of the foredeep, while the southern one was represented by the still undeformed Sakarya continental margin.

KEY-WORDS

Permian granitoids, slide-block, foredeep, Intrapontide suture, Taraklı Flysch, Turkey.

1. Introduction

Foreland basins represent a first-order tectonic element in the framework of collisional belts (e.g., Allen et al., 1986; DeCelles and Gilles, 1996). They originate during the first stage of collision when a passive margin collides with an active continental margin after the closure of an oceanic basin by subduction/obduction processes. One of the depo-zones of the foreland basin is represented by the foredeep, i.e. an elongate, deep sea-floor depression generally filled by turbidites, sometimes associated with debris flows and slide deposits, which are supplied by the advancing orogenic wedge or, to a lesser extent, by the peripheral bulge. In addition, turbidites supplied by extrabasinal, distal domains and transported parallel to the front of the advancing wedge can also be deposited in the foredeep.

The characteristics of these sediments provide useful insights for the reconstruction of the history of the collisional belt through time and space (e.g. Dickinson, 1988; Fedo et al., 2003; Carrapa, 2010). In this frame, the coarser grained deposits, like the slide-blocks, can be used to retrieve direct information on the source areas that surrounded the foredeep, providing valuable paleogeographic constraints.

The tectonic setting of Turkey (Fig. 1) can be described as a puzzle of amalgated continental microplates separated by ophiolite-bearing Tethyan sutures derived by the closure of different branches of oceanic basins whose ages range from Late Neoproterozoic to Late Cretaceous (e.g. Göncüoğlu et al., 1997; Okay and Tüysüz, 1999; Moix et al., 2008 and quoted references). The closure of these oceanic branches by subduction/obduction processes is followed by various stages of continental collision leading to the development of foredeeps that change their

shape, infilling mechanism and sediment types through time. One of these sutures is the Intrapontide suture (IPS) zone, located in the northern Turkey between the Sakarya (SK) and Istanbul-Zonguldak (IZ) continental terranes. In this suture zone, the foredeep deposits are represented by the Late Cretaceous - Middle Paleocene Taraklı Flysch deposited at the top of the SK terrane during the final stage of the continental collision between the SK and IZ continental margins (Catanzariti et al., 2013; Akbayram et al., 2016 and references therein). Until now, the scenario during this late stage collision has not been reconstructed in detail, because the original tectonic setting of the IPS zone has been strongly reworked by the active strike-slip North Anatolian Shear Zone (NASZ; Şengör et al., 2005; Ellero et al., 2015a). However, useful information on this scenario can be obtained by the analysis of the coarse-grained deposits occurring in the Taraklı Flysch, these can shed light on the nature of the domains that were surrounding the foredeep during the deposition of the Taraklı Flysch.

In this paper, we have studied the petrography and determined the U-Pb age of plutonic rocks found as an exotic block in the Late Cretaceous - Paleocene Taraklı Flysch from the Boyalı area (Fig. 1) in northern Anatolia. In order to identify the source area of this intrusive body, its age and first-order petrographic characteristics are compared with other plutonic rocks described in both the SK and IZ tectonic terranes.

It is important to highlight that in both the SK and IZ terranes the intrusive ages of granitoid rocks cover a wide age interval. The oldest granitoids are those of Neoproterozoic age found in the IZ terrane (Ustaömer et al., 2016) whereas the SK terrane is characterized by granitoids showing Devonian and Carboniferous ages

(Okay et al, 1996; Ustaömer et al, 2012; Karslı et al, 2016; Okay and Topuz, 2017; Aysal et al., 2017). However, rocks with similar ages have not been recognized in the IZ terrane. Particularly interesting are the Permo-Triassic intrusive rocks that have been reported in the IZ terrane (Aysal et al., 2018 and references therein). Permo–Triassic magmatic zircons have been recognized as fragments in the Triassic metasedimentary rocks from the Karakaya Complex sandstones (SK terrane, Ustaömer et al., 2016), but an in-place granite body has not been noticed yet. In addition, Middle Jurassic age has been got by both granites from IZ (Cimen et al., 2017) and SK (Okay et al., 2014) terranes. Recently, Karsli et al. (2018) have obtained a Late Cretaceous age from granites intruded into the SK terrane.

Thus, the resulting age of the granitoids, together with a review of the main stratigraphic features of the Taraklı Flysch, can allow a better understanding on the final stage of the continental collision, as, for instance, the features of the orogenic wedge at the border of the foredeep.

2. The Intrapontide suture zone: geological background

The tectonic setting of Turkey (Fig. 1) is characterized by several Paleo- and Neo-Tethys suture zones that are distributed around several continental terranes of both Gondwana- and Laurasia-origin (Şengör and Yilmaz, 1981; Okay and Tüysüz, 1999; Robertson, 2002; Moix et al., 2008; Göncüoğlu, 2010). This tectonic setting is the result of a long-lived geodynamic history of Mesozoic age and is originated by the complex interplay between small continental microplates and wide oceanic areas, all

located between the continental margins of two megaplates, the Gondwana to the south and the Laurasia to the north (Stampfli and Borel, 2002; Stampfli and Kozur, 2006). These oceanic areas were originated and subsequently destroyed by subduction and obduction processes leading to multiple continental collisional events whose record is partially preserved in the suture zones.

The northernmost suture zone preserved in Turkey is the IPS zone, an east-west trending assemblage of deformed and metamorphosed continental and oceanic units running from the Aegean coast to the central Anatolia (e.g. Şengör and Yılmaz, 1981; Okay and Tüysüz, 1999; Göncüoğlu et al., 2008; Hippolyte et al., 2016; Marroni et al., 2014; Frassi et al., 2016; Okay et al., 2017). The units of IPS zone are thrust by the IZ continental terrane and both are, in turn, thrust over the SK continental terrane through a N-dipping subduction planes. However, the pristine tectonic relationships of these units with the continental terranes are strongly modified since Early Eocene by the brittle tectonics related to the NASZ (Ottria et al., 2017 and references therein). Owing to the occurrence of NASZ-related tectonics, we prefer the definition of the IZ and SK terranes instead of IZ and SK zones, that we use only to describe the paleogeography (e.g. Ocakoğlu et al., 2018).

The most relevant feature of the IPS zone is the occurrence of oceanic units deformed and metamorphosed under HP-LT conditions known as Daday, Saka and Domuz Dağ Units (Okay et al., 2006, 2013; Marroni et al., 2014; Aygül et al., 2015a; Frassi et al., 2018). These units, that are grouped in the Central Pontide Structural Complex (CPSC, e.g. Tekin et al, 2012; Frassi et al., 2016) also known as the Central Pontides Supercomplex (e.g. Okay et al., 2013), consist of an assemblage of slices of metasedimentary rocks, metabasites and metaserpentinites showing different

metamorphic imprint. The highest metamorphism is shown by the Domuz Dağ Unit (Okay et al., 2006) that is characterized by eclogites, garnet- and glaucophane-bearing amphibolites and albite- and chlorite-bearing schists. The $^{40}Ar/^{39}Ar$ dating by Aygül et al. (2016) indicates that the eclogite facies peak metamorphism took place in the earliest Late Jurassic. The Saka Unit (Okay et al., 2013) includes instead garnet-bearing amphibolites, garnet-bearing micaschists and coarse-grained impure marbles. The garnet-bearing amphibolites are affected during the Late Jurassic (Marroni et al., 2014) by a peak metamorphism developed at P/T conditions coherent with an HP epidote-amphibolite facies. The Daday Unit (Frassi et al., 2018) includes slices of metabasites, quartzites, micaschists and paragneisses affected by blueschist facies metamorphism of Late Jurassic age (Frassi et al., 2018). In addition, a further tectonic unit known as the Emirköy Unit (Aygül et al., 2015a; Frassi et al., 2018) represented by a monotonous succession of metaturbidites affected by low-grade metamorphism can be also regarded as derived from the same oceanic domain from which the HP metamorphic units originated.

The oceanic units occurring in the IPS zone indicate that a large oceanic area, known as the Intrapontide Ocean basin, existed since Triassic between the SK and the IZ continental margins (Şengör and Yılmaz, 1981; Göncüoğlu et al., 1987, 2008, 2012, 2014; Yılmaz, 1990; Göncüoğlu and Erendil, 1990; Robertson et al., 1991; Okay et al., 1996; Yılmaz et al., 1997; Okay and Tüysüz, 1999; Okay, 2000; Robertson and Ustaömer, 2004; Akbayram et al., 2013; Marroni et al., 2014; Frassi et al., 2018). The Intrapontide Ocean basin was progressively closed by subduction during the Jurassic to Late Cretaceous time span (Okay et al., 2006, 2013; Marroni et al., 2014; Aygül et al., 2015a; Frassi et al., 2018). In this framework, the Daday, Saka, Domuz Dağ and

Emirköy Units represent fragments of a supra-subduction oceanic crust (Sayit et al., 2016) deformed and metamorphosed within an accretionary wedge at different depths corresponding to different P-T paths and different peak metamorphic conditions, from eclogite to blueschist and greenschist facies. The structural and geochronological data (Okay et al., 2006; 2013; Marroni et al., 2014; Aygül et al., 2015a; Frassi et al., 2018) indicate that these units experienced underthrusting and accretion in the Late Jurassic - Early Cretaceous and then were subjected to exhumation from the Early Cretaceous up to the Paleocene.

These units are associated with non-metamorphic Late Jurassic ophiolites and ophiolite-bearing sedimentary mélanges of Late Cretaceous age (Arkotdag and Kızılırmak mélanges; Tokay, 1973, Göncüoğlu et al., 2012, 2014; Çelik et al., 2016). Their ages and the occurrence of continental- and oceanic-derived blocks therein suggest an origin of these mélanges during the final phase of closure of the Intrapontide Ocean basin (Tokay, 1973; Göncüoğlu et al., 2014; Aygül et al., 2015a; Frassi et al., 2016). The final closure of this oceanic basin is still matter of debate, but several authors have proposed a closure at the end of the Late Cretaceous (Göncüoğlu et al., 2014; Ocakoğlu et al., 2018).

Additional evidence supporting the closure of the Intrapontide Ocean basin are provided by the remnants of volcanis arc of Late Cretaceous age that have been recognized within the tectonic units known as Kösedağ Metavolcanic Complex and Tafano Unit (Ellero et al., 2015b; Aygül et al., 2015b). Differently, remnants of volcanic and plutonic rocks of Middle Jurassic age crop out in the northern areas of the IPS zone within the Geme, Devrekani, Küre and Çangaldağ Metamorphic complexes (Okay et al., 2014; Çimen et al., 2017, 2018).

The tectonic units from the IPS zone are thrust over the SK continental terrane that consists of a Variscan continental basement associated with a strongly deformed and metamorphosed subduction complex known as Karakaya Complex (Okay et al., 2002; Okay and Göncüoğlu, 2004; Sayit and Göncüoğlu, 2013). The Karakaya Complex consists of a deformed and metamorphosed Triassic subduction-accretion complex comprising blueschist to eclogite facies metamorphic rocks of Late Triassic age (Okay and Monié 1997; Okay et al., 2002). This metamorphism is related to the "Cimmerian orogeny" leading to a deformed and metamorphosed belt resulting by the subduction of the Paleo-Tethys oceanic lithosphere below the Laurasia continental margin (Şengör and Yılmaz, 1981). The Variscan basement as well as the Karakaya Complex are unconformably covered by Early Jurassic to Late Cretaceous, continental deep-marine sedimentary succession passing upward to turbidites (here reported as Taraklı Flysch), regarded as a foredeep deposits ranging in age from Early Maastrichtian to Middle Paleocene (Catanzariti et al., 2013).

In turn, the IZ terrane includes a Neoproterozoic basement (e.g. Ustaömer and Rogers, 1999) unconformably overlain by a very thick sedimentary sequence whose age spans from Ordovician to Carboniferous (e.g. Görür et al., 1997). Such a Paleozoic sequence is unconformably overlain by a thick sequence of Late Permian-Triassic continental clastic deposits topped by Middle to Late Jurassic carbonate deposits, which are covered by Late Cretaceous-Paleocene turbidite deposits interleaved with andesitic volcanic flows (e.g. Dizer and Meriç, 1983; Aydın et al., 1986).

From this picture the Paleocene epoch can be regarded as the time when the collision between IZ and SK terranes occurred (Catanzariti et al., 2013). In this framework, the Taraklı Flysch deserves special attention mainly because it can

provide useful insights on the ultimate stage of collision (e.g. Akbayram et al, 2016; Ocakoğlu et al., 2018).

3. Geology of the study area

3.1 Geological setting

The studied section of the Taraklı Flysch is located in the Boyalı area, northern Anatolia along the Akçay Valley between the Bahçecik and Boyalı Villages (Fig. 2a). This valley shows an east-west trend and its northern flank is delimited by the Aylı Dağ Mountain.

In this area the tectonic setting is dominated by the deformation related to the NASZ which affected a tectonic stacking characterized by three imbricate units belonging to the IPS zone, namely the ophiolite Aylı Dağ Unit (Göncüoğlu et al., 2012), the Arkot Dağ Mélange (Göncüoğlu et al., 2014) and the Daday Unit (Frassi et al., 2018), that are thrust all together over the SK terrane (Catanzariti et al., 2013; Ellero et al., 2015a) (Fig. 2a and b). In this area, the SK terrane displays a stratigraphic log that includes continental- to shallow-marine Early Jurassic clastic rocks that are disconformably overlain by the Middle Jurassic to Early Cretaceous neritic limestones (Altıner et al., 1991). The neritic limestones are unconformably overlain by the Early to Late Cretaceous pelagic limestones showing a transition to turbidite deposits of the Taraklı Flysch (Early Maastrichtian to Middle Paleocene). The age of the Taraklı

Flysch has been discussed by Catanzariti et al. (2013) using nannofossils collected in the Bahçecik and Boyalı area.

South of Boyalı village (Fig. 2a), the Taraklı Flysch is imbricated with slices of the Tafano Unit (Ellero et al., 2015b) probably as a result of the strike-slip tectonics of the NASZ. The Tafano Unit consists of a Late Cretaceous sequence including a volcanic complex covered by sedimentary succession. The volcanic rocks, that display basaltic and basaltic-andesitic compositions with sub-alkaline affinities, are associated with volcaniclastic deposits evolving to late Santonian-middle Campanian marly-calcareous turbidites (Ellero et al., 2015b).

In addition, a small klippe of the IZ terrane consisting of Devonian deposits has been identified between two NE-SW striking strike-slip faults at the top of the Arkot Dağ Mélange, west of the Ayli Dağ Mountain (Fig. 2a).

The relationships among these units are sealed by the Late Paleocene-Eocene deposits of the Safranbolu-Karabük Basin (Fig. 2a) that widely crop out in the western part of the Akçay Valley (Uğuz et al., 2002). Thus, the relationships between the tectonic units of the IPS zone and the SK and IZ terranes can be regarded as the result of the pre-Eocene tectonic events.

3.2 Stratigraphic features

The stratigraphy of the Taraklı Flysch (Fig. 3a) has been reconstructed by Catanzariti et al. (2013) in the sections cropping out along the northern side of the Akçay Valley, between the Bahçecik and Boyalı Villages and along the Boyalıçay Valley. In this study we have expanded the field survey of Catanzariti et al. (2013), mapping the western extent of the Akçay Valley (Fig. 2c).

The thickness of the Taraklı Flysch is at least 700 m and shows a thickening and coarsening upward (Fig. 3a). According to Catanzariti et al. (2013) it can be divided into five different lithofacies that, from bottom to top, are: "thin-bedded turbidites", "medium-grained arenites", "conglomerates", "calcareous coarse-grained turbidites" and "slide-blocks in shaly-matrix" (Fig. 3b). In the study area the "calcareous coarse-grained turbidites" facies is not present while the conglomerates facies is well developed.

The about 400 m thick thin-bedded turbidites facies consists of thin to medium laterally continuous beds. The strata are made of medium- to fine-grained arenites passing to coarse-grained siltites (Fig. 3c). These strata are well graded low density turbidites (coinciding with F9a facies of Mutti, 1992) and current ripples and sinusoidal lamina are common.

The medium-grained arenites lithofacies is characterized by up to 70 m thick sequence of turbidites represented by 0.4-2 m thick beds of amalgamated medium- to fine-grained arenites (Fig. 3d). These strata are characterized by a massive structure and they can be compared with the F8 facies of Mutti (1992). The bottom surface of these strata is characterized by sole marks and by the common presence of organic matter.

A thick level of well rounded clast- to matrix-supported conglomerates (mainly F3 facies of Mutti, 1992) characterizes the medium part of the Taraklı Flysch (Fig. 3e). These strata are associated with coarse-grained high density turbidity current deposits. Thick to medium beds without internal structures and with poor sorting are the most common facies. The “conglomerates” lithofacies is characterized by granitoids-dominated composition of the pebbles while the carbonatic clasts are

rare. These beds, derived from high density erosive flows probably connected to a coarse-grained river-delta systems.

The upper part of the succession, which is more than 300 m thick, is dominated by slide-blocks embedded in a fine grained-matrix (Fig. 3f). The matrix of this lithofacies is characterized by varicolored mainly shaly to silty deposits. The slide-blocks, usually with lenticular shapes, have variable composition and sizes ranging from meter-sized boulder up to more than 100 m-thick blocks. Even if the primary relationships between the slide-blocks and the surrounding matrix are always tectonized, their emplacement due to submarine landslides is suggested by syn-sedimentary deformation structures recognized in the sediments surrounding the blocks and by slide-block-derived monomict pebbly-mudstones and pebbly-sandstones that are present around several slide-blocks. The slide-blocks are mainly granitoids (Fig. 3g), orthogneisses, metagabbros amphibolites, Jurassic carbonatic turbidites as well as Ordovician quartzarenites, black shales, crinoidal and brachiopod-bearing Devonian-Carboniferous limestones and probably Triassic red quartz-arenites which are typical compounds of the IZ terrane. As indicated in the geological scheme of Fig. 2a, the granitoids blocks are the most common and those cropping out between the villages of Boyalı and Bahcecik and, to a lesser extent between Boyalı and Bayramören villages can be mapped at 1:10.000 scale. Within the individual slide-blocks of plutonic rocks primary relationships among different magmatic lithofacies can be recognized. These slide-blocks can be regarded as “exotic” according to the lacking of the occurrence of similar lithologies in the units cropping out in the surrounding area (Uğuz et al., 2002; Catanzariti et al., 2013).

We have sampled a large intrusive exotic block that, as illustrated in the geological map of Fig. 2c, covers an area of ca. 9 km^2. In " 5. Results" section the petrographical features of this block as well as its zircon U-Pb age will be presented and discussed in relation to granitoids occurring in various terranes surrounding the IPS zone.

4. Analytical methods

Zircons were extracted from their host rocks (i.e. the intrusive exotic block of the Taraklı Flysch sampled in the Boyalı area) at the University of Geneva (Switzerland) by standard crushing, gravimetric- and magnetic-separation techniques. Approximately 200 zircon crystals were selected from 3 of the 15 hand samples collected. These crystals were hand-picked under a binocular microscope and mounted in epoxy resin. The mounts were polished to expose the crystal interior domains and imaged by cathodoluminescence using a JEOL JSM-7001F Schottky scanning electron microscope at the University of Geneva.

In-situ zircon U-Pb isotope analyses were performed at the Institute of Earth Sciences of the University of Lausanne (Switzerland) using a Thermo ELEMENT XR sector field ICP-MS coupled with a Resolution 193 nm Excimer laser ablation system. Data were acquired in time-resolved, peak-jumping, pulse-counting mode utilizing a routine where 30 seconds of background measurement were followed by 30 seconds of sample ablation. Laser induced fractionation of Pb and U was minimized during analysis by employing a soft ablation regime using a repetition rate of 5 Hz and an energy density of ~3 J/cm^2 per pulse. Laser spot sizes were 30 µm. The measurement

protocol and the parameters of mass spectrometer optimization follow Ulianov et al. (2012). Laser-induced elemental fractionation and instrumental mass discrimination were corrected by normalization to the reference zircon GJ-1. To test the accuracy and external reproducibility of the obtained age data, the Plešovice reference zircon (Sláma et al., 2008) was measured after every ~ 8 unknowns and the data are presented in Table 1. The Plešovice secondary standard gave a weighted mean age of 337.5 ± 0.6 Ma (2SD, n = 21; MSWD = 0.66). The calculated age is consistent, within uncertainty, with the ID-TIMS value reported by Sláma et al. (2008). All raw data from Lausanne was processed using the LAMTRACE software package (Jackson, 2008) and no common Pb correction was applied due to the presence of trace ^{204}Hg in the Ar gas. Common Pb was dealt with monitoring ^{201}Hg, ^{204}(Hg+Pb) as well as (^{204}Pb+^{204}Hg)/^{206}Pb ratios. The homogeneity of the ablated material was confirmed by monitoring the ^{206}Pb/^{238}U and ^{207}Pb/^{235}U vs. time spectra, and fluctuations in these ratios were interpreted to represent mixing between different age domains within the crystals. Spectra with mixed domains were subsequently discarded.

5. Results

5.1 Field data and petrography

We have sampled a large-block of granitoids that, as illustrated in the geological map of Fig. 2b, occurs as a square body and it is cut, in its northern side, by an E-W trending strike-slip fault. The granitoids are well exposed along the Akçay river where two different facies were recognized (Fig. 4a).

The main, melanocratic facies (Fig. 4b) is located in the upper part of the block and consists of an isotropic medium-grained quartz-monzonites (Fig. 4c) with phenocrysts of amphibole representing the dominant rock-forming phase forming up to ca. 50 vol% of the rock assemblage. The quartz-monzonites contain plagioclase, K-feldspar and widespread quartz, titanite as well as primary iron-rich epidote. A minor amount of chlorite replacing former biotite crystals is also observed. Other common accessory phases are apatite, magnetite and zircon. This most voluminous facies is intruded by a second leucocratic unit (Fig. 4d) that occurs in the lower part of the slide-block. This facies is made of coarse-grained leucocratic granodiorites (Fig. 4e) with crystals of K-feldspar, quartz and plagioclase reaching up to 5 cm in size. Mirmekitic textures are common in some of the analyzed thin sections. Biotite is the main mafic phase in the rock, forming less than 5 vol% of the granodiorites. The biotite crystals are pervasively altered to iron-rich chlorites. Accessory phases are titanite, reaching up to 1 mm in size, epidote (i.e. pistacite), apatite and zircon. In thin section, both lithofacies are cross-cut by secondary calcite veins. The plagioclase in the quartz-monzonites is commonly pervasively altered to sericite. Dykes of the leucocratic granodiorites cut the quartz-monzonites (Fig. 4f) whereas the latter form enclaves that are recognized along the contact zone between the two units. Finally, both the lithotypes are cross-cut by fine-grained aplitic dykes.

5. 2 Zircon texture and U-Pb geochronology

Zircon were extracted from three samples (Fig. 5), two from the quartz-monzonites (i.e. TC316a and TC316b) and one from the leucocratic granodiorites (TC319). Zircon crystals from both lithofacies are subhedral to euhedral and reach up to 350 µm in

length. Under cathodoluminescence (CL), most of the grains from the quartz-monzonites are characterized by the occurrence of CL-dark homogeneous or faintly zoned centres surrounded by fine-scale oscillatory zoned rims. The centres commonly exhibit evidence of resorption that can be fractured and occasionally metamictic (Fig. 5). Most of zircon grains from the leucocratic granodiorites exhibit complex core-to-rim growth zoning with common local intermediate resorption features that allows to distinguish centres and rims (Fig. 5). A subset of zircon crystals from both rock-types are homogeneous under CL, either bright or dark.

Seventy-two zircon crystals were dated by LA-ICP-MS U-Pb analysis. The complete dataset is provided in Table 1. In Fig. 6, concordia diagrams and weighted average plots are shown. The analyses performed on both centres and rims yield apparent spot ages that vary from 270 to 232 Ma, with most of the data forming a cluster at ca. 260 Ma. Most of the spot analyses are discordant and only twenty-three analyses passed the <10% discordancy test (Conc.(%) in Tab. 1). Zircons from the two quartz-monzonites samples yielded weighted average $^{206}Pb/^{238}U$ ages of 261.0 ± 1.6 Ma (n=16, MSWD = 0.5) and 258.3 ± 2.1 Ma (n=15, MSWD = 1.2). Zircon spot ages from the leucocratic granodiorites are more scattered giving a weighted average $^{206}Pb/^{238}U$ age of 256.8 ± 2.8 Ma (n=18, MSWD = 3.1). These three calculated ages are the same within the error limits. Considering only the sub-concordant spot analyses of the three sample together, the weighted mean gives a $^{206}Pb/^{238}U$ age of 260.8 ± 2.2 Ma. This is considered to be the formation age of the intrusive body.

6. Discussion

6.1 Occurrence of slide-blocks of Late Permian granitoids in the Taraklı Flysch

The succession of the Taraklı Flysch cropping out in the Boyalı area (Fig. 3a) shows all the features of syn-tectonic sedimentation in a foredeep environment with a clear thickening and coarsening upward evolution from thin-bedded turbidites to medium-grained arenites and calcareous coarse-grained turbidite lithofacies (Catanzariti et al., 2013). This succession ends with a level of slide-blocks in shaly-matrix lithofacies, that can be considered as the result of fast and catastrophic sedimentary event that predate the closure of the basin and its deformation. This catastrophic event originated by the instability of the front of the orogenic wedge probably triggered by earthquakes induced by the underthrusting of a lower plate with rugged morphology, as detected in modern and fossil foredeep and trench deposits (Festa et al., 2010 and quoted references). The slide-blocks are sourrounded by monomict pebbly-mudstones and pebbly-sandstones that show synsedimentary deformational structures. The largest slide-block consists of the plutonic rocks described in this paper. This slide block is surrounded by smaller blocks made up by the same rocks as the largest one (Fig. 2c). These lines of evidence suggest that all the slide-blocks derived from a source area that was located close to the foredeep where the Taraklı Flysch sedimented. Thus, this source area can be identified either in the front of the advancing orogenic wedge or, alternatively, in the peripheral bulge, being the only settings that are able to provide coarse-grained deposits in the upper part of the Taraklı Flysch. In the first hypothesis, the source area of the slide-blocks of granitoids is represented by IZ terrane, whereas in the second one the same role is played by the SK terrane.

6.2 Felsic plutonic rocks in the SK and IZ terranes

Undeformed plutonic rocks of Paleozoic age occur in both the SK and IZ terranes (Aysal et al., 2018 and references therein). In the SK terrane, most of the metamorphosed granitoids are Devonian in age and crop out in the western part of the Sakarya zone as tectonic slices generally occurring within the Triassic subduction-accretion complexes (Karakaya Complex, Okay et al., 1996, 2006; Aysal et al., 2012a; 2012b; Sunal, 2012). These intrusives, which are mainly granodiorites, monzogranites and monzodiorites show geochemical and petrographic features of continental arc magmas (Aysal et al., 2012a; 2012b). In the SK terrane Carboniferous-Early Permian granitoids are also common and widespread intruding the LP-HT metamorphic rocks cropping out in Central Sakarya (Söğüt granite, Ustaömer et al., 2012) and Eastern Pontide (Topuz et al, 2010; Kaygusuz et al., 2012; Ustaömer et al., 2013) areas. The U-Pb zircon ages of these granitoids, which exhibit both high K I- and S-type signatures, range from 327-324 in Central Sakarya and to 303-325 Ma in the Eastern Pontide. Therefore the age of the intrusive rocks cropping out in the SK terrane does not match with the age of the exotic block in the upper part of the Taraklı Flysch.

In the IZ terrane the Paleozoic sequence is continuous from Ordovician to Carboniferous with no intervening phases of magmatism or deformation (e.g., Görür et al., 1997; Özgül, 2012). The Ordovician sedimentary rocks are underlain by Late Neoproterozoic granitoids (Ustaömer et al., 2005). The Late Neoproterozoic granitoids as well as the Paleozoic sedimentary sequence were deformed and metamorphosed during the Carboniferous and were subsequently intruded by syn-

and post-tectonic Late Carboniferous and Permian granitoids (Yılmaz et al., 2012; Aysal et al., 2017; 2018). These intrusive rocks show a wide range of ages from 309 to 235 Ma similar to the plutonic rocks described in the Strandja massif, Istanbul area and central Pontides (Ustaömer et al., 2005; Sunal et al., 2006; Şahin Yılmaz et al., 2014; Machev et al., 2015; Aysal et al., 2018).

The Kürek granite, located in the IZ terrane only few kilometeres north of the studied exotic blocks in the Taraklı Flysch, has a Late Permian age of 262 ± 3 Ma (Okay et al., 2013) which overlaps with the age of the slide-block dated in this study. Therefore, this granitoid is considered to be the best candidate to represent the source of the slide-block in the Taraklı Flysch. It is worth noting that the Kürek granite and the slide-block also share similar petrographic features, with the former described by Okay et al. (2013) as a composite pluton consisting of hornblende-bearing diorites intruded by granites-granodiorites. The Kürek granites occur at the top of the metamorphic oceanic units belonging to the IPS zone. This tectonic position suggests that the Kürek granites can be interpreted as a klippe belonging to the southernmost part of the IZ terrane, subsequently dislocated by the strike-slip tectonics related to the NASZ (Ellero et al., 2015a; Ottria et al., 2017).

6.3 Potential source area of slide-blocks in the Taraklı Flysch

The age and the petrography of the granitoids in the Taraklı Flysch match with those of granitoids derived from the IZ terrane. Differently from SK terrane, the IZ one hosts Late Carboniferous to Permian granitoids that crop out also in the Central Pontides. A klippe of IZ terrane, consisting of Devonian sedimentary rocks, occurs 5 km north of the study area whereas another klippe, still belonging to the IZ terrane,

occurs farther away, at about 25 km northward. This klippe consists of granitoids (Kürek granite) showing similar petrography and the same age of the rocks studied in this paper. As previously stated, these klippe can be regarded as the remnants of the southernmost part the IZ terrane, subsequently dismembered and isolated by the strike-slip tectonics.

Our data also suggest that the slide-blocks of granitoids derived from the advancing front of the IZ terrane that was located at the top of the orogenic wedge. This wedge was bounded southward by a foredeep where the Taraklı Flysch deposited. Another evidence comes from the occurrence of crinoidal and brachiopod-bearing Devonian-Carboniferous limestones and Triassic red quartzarenites found as slide-blocks in the uppermost part of the Taraklı Flysch (Catanzariti et al., 2013). Devonian limestone blocks together with blocks of Neoproterozoic crystalline rocks are also reported from the Late Cretaceous-Paleocene “Bakacak Olistostrome” in Armutlu Peninsula on the western continuation of the IPS (Göncüoğlu et al, 1987; Akbayram et al, 2013). These lithologies are found only in the IZ terrane.

In this reconstruction, the IZ terrane can be regarded as a wide nappe that thrust over the IPS units reaching the rim of the foredeep. The slide-block of granitoids were then detached from the IZ terrane, emplaced by slide in the foredeep and interposed within the turbidites of the Taraklı Flysch. Conversely, the opposite side of the foredeep is represented by the SK continental margin, not still affected by deformation, that represents the source area for the thin-bedded turbidites of the Taraklı Flysch. A reconstruction of the depositional setting of the Taraklı Flysch is proposed in the Fig. 7.

7. Conclusion

1. The top of the Taraklı Flysch is characterized by a level of slide-blocks in shaly-matrix lithofacies, that can be considered as the fast catastrophic event that predates the closure of the basin and its deformation.
2. Among the slide-blocks, the largest one consists of intrusive rocks of Late Permian age by U/Pb geochronology.
3. According to the available regional data, these "exotic" granitoids are derived from the IZ terrane, where Late Permian granites are widespread.
4. This evidence suggests a new picture where the slide-blocks of granites are supplied from the advancing front of the IZ terrane located at the top of the orogenic wedge that bounded northward the foredeep.
5. This picture is coherent with thrusting of the IZ terrane over the IPS units across the whole extension of the IPS zone during the continental collision and before the inception of the NASZ.

Acknowledgments

The research has been funded by PRA of University of Pisa. This research benefits also by grants from Darius Project and PRIN 2010-11 projects (resp. M. Marroni). F. Farina wishes to acknowledge the financial support received from the European Union's Horizon 2020 research and innovation program under the Marie Skłodowska-

Curie grant agreement No 701494. We would like to thank A.I Okay and N. Aysal, I. Uysal and an anonymous referee for their constructive reviews.

References

Akbayram, K., Okay, A. I. , Satır, M., 2013. Early Cretaceous closure of the Intra-Pontide Ocean in western Pontides (northwestern Turkey). Journal of Geodynamics 65, 38-55.

Akbayram, K., Şengör, A.M.C., Özcan, E., 2016. The evolution of the Intra-Pontide suture: Implications of the discovery of Late Cretaceous-Early Tertiary mélanges. In: Sorkhabi, R. (Eds.), Tectonic Evolution, Collision, and Seismicity of Southwest Asia: In Honor of Manuel Berberian's Forty-Five Years of Research Contributions, Geological Society of America Special Papers 525, doi:10.1130/2016.2525(18).

Allen, P.A., Homewood, P., Williams, G.D., 1986. Foreland basins: an introduction. Foreland basins. International Association of Sedimentologists, Special Publication 8, 3-12.

Altıner, D., Koçyigit, A., Farinacci, A., Nicosia, U., Conti, M.A., 1991. Jurassic-Lower Cretaceous stratigraphy and paleogeographic evolution of the southern part of northwestern Anatolia. Geologica Romana 27, 13-80.

Aydın, M., Sahintürk, O., Serdar, H.S., Özçelik, Y., Akarsu, I., Üngör, A., Çokuğraş, R., Kasar, S., 1986. The geology of the area between Ballidağ and Çangaldağ (Kastamonu). Bulletin of the Geological Society of Turkey 29, 1-16.

Aygül, M., Okay, A.I., Oberhansli, R., Ziemann, M.A., 2015a. Thermal structure of low-grade accreted Lower Cretaceous distal turbidites, the Central Pontides, Turkey: insights for tectonic thickening of an accretionary wedge. Turkish Journal of Earth Sciences 24, 461-474.

Aygül, M., Okay, A.I., Oberhansli, R., Schmidt, A., Sudo, M., 2015b. Late Cretaceous infant intra-oceanic arc volcanism, the Central Pontides, Turkey: petrogenetic and tectonic implications. Journal of Asian Earth Sciences 111, 312-327.

Aygül, M., Okay, A.I., Oberhansli, R., Sudo, M., 2016. Pre-collisional accretionary growth of the southern Laurasian active margin, Central Pontides, Turkey. Tectonophysics 671, 218-234.

Aysal, N., Ustaömer, T., Öngen, S., Keskin, M., Köksal, S., Peytcheva, I., Fanning, M., 2012a. Origin of the Early-Middle Devonian magmatism in the Sakarya Zone, NW Turkey: Geochronology, geochemistry and isotope systematics. Journal of Asian Earth Sciences 45, 201-222.

Aysal, N., Öngen S., Peytcheva, I., Keskin, M., 2012b. Origin and evolution of the Havran Unit, Western Sakarya basement (NW Turkey): new LA-ICP-MS U-Pb dating of the metasedimentary-metagranitic rocks and possible affiliation to Avalonian microcontinent. Geodinamica Acta 25, 226-247.

Aysal, N., Keskin, M., Peytcheva, I., Durum O., 2017. Geochronology, geochemistry and isotope systematics of a mafic-intermediate dyke complex in the Istanbul Zone. New constraints on the evolution of Black Sea. Geological Society of London, Special Publications, 464.

Aysal, N., Yılmaz Şahin, S., Güngö, Y., Peytcheva, I., Öngen, S., 2018. Middle Permian-Early Triassic magmatism in the Western Pontides, NW Turkey: Geodynamic signicance for the evolution of the Paleo-Tethys. Journal of Asian Earth Sciences 164, 83-103.

Carrapa, B., 2010. Resolving tectonic problems by dating detrital minerals. Geology 38(2), 191-192.

Catanzariti, R., Ellero, A., Göncüoğlu, M.C., Marroni, M., Ottria, G., Pandolfi, L., 2013. The Taraklı Flysch in the Boyalı area (Sakarya Terrane, northern Turkey): implications for the tectonic history of the IntraPontide suture Zone. Comptes Rendus Geoscience 345, 454-61.

Çelik, Ö.F., Chiaradia, M., Marzoli, A., Özkan, M., Billor, Z., Topuz, G., 2016. Jurassic metabasic rocks in the Kızılırmak accretionary complex (Kargı region, Central Pontides, Northern Turkey). Tectonophysics 672/673, 34-49.

Çimen, O., Göncüoğlu, M.C., Simonetti, A., Sayit, K., 2017. Whole rock geochemistry, Zircon U-Pb and Lu-Hf isotope systematics of the Çangaldağ Pluton: Evidences for Middle Jurassic continental arc magmatism in the Central Pontides, Turkey. Lithos 290-291, 136-158.

Çimen, O., Göncüoğlu, M.C., Simonetti, A., Sayit, K., 2018. New zircon U-Pb LA-ICP-MS ages and Hf isotope data from the Central Pontides (Turkey): Geological and geodynamic constraints. Journal of Geodynamics 116,23-36.

DeCelles, P. G.,Giles, K. A., 1996. Foreland basin systems. Basin research 8(2), 105-123.

Dickinson, W. R., 1988. Provenance and sediment dispersal in relation to paleotectonics and paleogeography of sedimentary basins. In: Dickinson, W.R. (Eds.), New Perspectives in Basin Analysis. Springer, New York, 3-25.

Dizer, A., Meriç, E., 1983. Late Cretaceous-Paleocene stratigraphy in Northwest Anatolia. Maden Tetkik ve Arama Enstitutusu Dergisi 95/96, 149-163.

Ellero, A., Ottria, G., Marroni, M., Pandolfi, L., Göncüoğlu, M.C., 2015a. Analysis of the North Anatolian Shear Zone in Central Pontides (northern Turkey): Insight for geometries and kinematics of deformation structures in a transpressional zone. Journal of Structural Geology 72, 124-141.

Ellero, A., Ottria, G., Sayit, K., Catanzariti, C., Frassi, C., Göncüoğlu, M.C., Marroni, M., Pandolfi, L., 2015b. Geological and geochemical evidence for a Late Cretaceous continental arc in the Central Pontides, Northern Turkey. Ofioliti 40, 73-90.

Fedo, C. M., Sircombe K. N., Rainbird R. H., 2003. Detrital zircon analysis of the sedimentary record. Reviews in Mineralogy and Geochemistry 53(1), 277-303.

Festa, A., Pini, G.A., Dilek, Y., Codegone, G., 2010. Mélanges and mélange-forming processes: A historical overview and new concepts. International Geological Review 52(10-12), 1040-1105.

Frassi, C., Göncüoğlu, M.C., Marroni, M., Pandolfi, L., Ruffini, L., Ellero, A., Ottria, G., Sayit, K., 2016. The Intra-Pontide Suture Zone in the Tosya-Kastamonu area, Northern Turkey. Journal of Maps 12, 211-219.

Frassi, C., Marroni, M., Pandolfi, L., Göncüoğlu, M.C., Ellero, A., Ottria, G., Sayit, K., Mcdonald, C.S., Balestrieri, M.L., Malasoma, A., 2018. Burial and exhumation history of the Daday Unit (Central Pontides, Turkey): implications for the closure of the Intra-Pontide oceanic basin. Geological Magazine 155(2), 356-376.

Göncüoğlu, M.C., 2010. Introduction to the Geology of Turkey: Geodynamic evolution of the Pre-Alpine terranes. General Directorate of Mineral. Res. Explor., Monography Series 5, 1-66.

Göncüoğlu, M.C., Erendil, M., 1990. Pre-Late Cretaceous tectonic units of the Armutlu Peninsula. Proceed. 8th Turkish Petrological Congress 8, 161-168.

Göncüoğlu, M.C., Erendil, M., Tekeli, O., Aksay, A., Kuscu, A., Ürgün, B., 1987. Geology of the Armutlu Peninsula. IGCP-5 Guide Book for the field excursion along Western Anatolia, Turkey, Ankara 5, 12-18.

Göncüoğlu, M.C., Dirik, K., Kozlu, H., 1997. General Characteristics of Pre-Alpine and Alpine Terranes in Turkey: Explanatory notes to the terrane map of Turkey. Annales Geologique de Pays Hellenique 37, 515-536.

Göncüoğlu, M.C., Gürsu, S., Tekin, U.K., Koksal, S., 2008. New data on the evolution of the Neotethyan oceanic branches in Turkey: Late Jurassic ridge spreading in the Intra-Pontide branch. Ofioliti 33, 153-164.

Göncüoğlu, M.C., Marroni, M., Sayit, K., Tekin, U.K., Ottria, G., Pandolfi, L., Ellero, A., 2012. The Aylı Dağ ophiolite sequence (central-northern Turkey): A fragment of Middle Jurassic oceanic lithosphere within the Intra-Pontide suture zone. Ofioliti 37, 77-91.

Göncüoğlu, M.C., Marroni, M., Pandolfi, L., Ellero, A., Ottria, ö., Catanzariti, R., Tekin, U.K., Sayit, K., 2014. The Arkot Dağ Mélange in Araç area, central Turkey:

Evidence of its origin within the geodynamic evolution of the Intra-Pontide suture zone. Journal of Asian Earth Sciences 85, 117-139.

Görür, N., Monod, O., Okay, A.I., Şengör, A.M.C., Tüysüz, O., Yiğitbaş¸ E., Sakinç, M., Akkök, R., 1997. Palaeogeographic and tectonic position of the Carboniferous rocks of the western Pontides (Turkey) in the frame of the Variscan belt. Bulletin de la Société Géologique de France 168, 197-205.

Hippolyte, J.-C., Espurt, N., Kaymakci, N., Sangu, E., Müller, C., 2016. Cross-sectional anatomy and geodynamic evolution of the Central Pontide orogenic belt (northern Turkey). International Journal of Earth Sciences 105(1), 81-106.

Jackson, S., 2008. LAMTRACE data reduction software for LA-ICP-MS. In: Sylvester P. (Eds.), Laser ablation-ICP-mass spectrometry in the Earth sciences: Current practices and outstanding issues. Mineralogical Association of Canada Short Course Series 40, 305-307.

Karslı, O., Dokuz, A., Kandemir, R., 2016. Subduction-related late Carboniferous to Early Permian magmatism in the eastern Pontides, the Camlik and Casurluk plutons: insights from geochemistry whole rock Sr-Nd and in situ Lu-Hd isotopes, and U-Pb geochronology. Lithos 266-267, 98-114.

Karsli, O., Aydin, F., Uysal, I., Dokuz, A., Kumral, M., Kandemir, R., Budakoglu, M., Ketenci, M., 2018. Latest Cretaceous “A2-type” granites in the Sakarya Zone, NE Turkey: Partial melting of the mafic lower crust in response to roll back of Neo-Tethyan oceanic lithosphere. Lithos 302-303, 312-328.

Kaygusuz, A., Arslan, M., Siebel, W., Sipah, F., Ilbeyli, N., 2012. Geochronological evidence and tectonic significance of Carboniferous magmatism in the southwest Trabzon area, eastern Pontides, Turkey. International Geology Review 54(15), 1-25.

Machev, P., Ganev, V., Klain, L., 2015. New LA-ICP-MS U-Pb zircon dating for Strandja granites (SE Bulgaria): evidence for two stage late Variscan magmatism in the internal Balkanides. Turkish Journal of Earth Sciences 24, 230-248.

Marroni, M., Frassi, C., Göncüoğlu, M.C., Di Vincenzo, G., Pandolfi, L., Rebay, G., Ellero, A., Ottria, G., 2014. Late Jurassic amphibolite-facies metamorphism in the Intra-Pontide Suture Zone (Turkey): an eastward extension of the Vardar Ocean from the Balkans into Anatolia? Journal of the Geological Society of London 171(5), 605-608.

Moix, P., Beccaletto, L., Kozur, H.W., Hochard, C., Rosselet, F., Stampfli, G.M., 2008. A new classification of the Turkish terranes and sutures and its implication for the paleotectonic history of the region. Tectonophysics 451, 7-39.

Mutti, E., 1992. Turbidite Sandstones. AGIP-Instituto di Geologia, Università di Parma, San Donato Milanese, 275 pp.

Ocakoğlu, F., Hakyemez, A., Açıkaliın, S., Altıner, S.Ö., Büyükmeriç, Y., Licht, A., Demircan, H., Şafak, Ü., Yıldiz, A., Yilmaz, I. Ö., Wagreich, M., Campbell, C., 2018. Chronology of subduction and collision along the Izmir-Ankara suture in Western Anatolia: records from the Central Sakarya Basin. Int. Geol. Rev. http://doi.org/10.1080/00206814.2018.1507009.

Okay, A.I., 2000. Was the Late Triassic orogeny in Turkey caused by the collision of an oceanic plateau? In: Bozkurt, E., Winchester, J.A., Piper, J.A.D. (Eds.), Tectonics and Magmatism in Turkey and surrounding Area. Geological Society of London, Special Publication 173, 25-41.

Okay, A.I., Göncüoğlu, M.C., 2004. The Karakaya complex: a review of data and concepts. Turkish Journal of Earth Sciences 13, 77-95.

Okay, A.I., Monié, P., 1997. Early Mesozoic subduction in the Easetern Mediterranean: evidence from Triassic eclogitie in the northwest Turkey. Geology 25, 595-598.

Okay, A.I., Topuz, G., 2017. Variscan orogeny in the Black Sea region. International Journal of Earth Sciences (Geol Rundsch) 106, 569-592.

Okay, A.I., Tüysüz, O., 1999. Tethyan sutures of northern Turkey. In: Durand, B., Olivet, J. L., Horvath, E., Serrane, M. (Eds.), The Mediterranean basins, extension within the Alpine Orogen. Turkish Journal of Earth Sciences 156. pp. 475-515.

Okay, A.I., Satır, M., Maluski, H., Siyako, M., Monie, P., Metzger, R., Akyüz, S., 1996. Paleo- and Neo-Tethyan events in northwest Turkey: geological and geochronological constraints. In: Yin, A., Harrison, M. (Eds.), Tectonics of Asia. Cambridge University Press, pp. 420-441.

Okay, A.I., Monod, O., Monié, P., 2002. Triassic blueschists and eclogites from northwest Turkey: vestiges of the Paleo-Tethyan subduction. Lithos 64, 155-178.

Okay, A.I., Satır, M., Siebel, W., 2006. Pre-Alpide orogenic events in the Eastern Mediterranean region. In: Gee, D.G., Stephenson, R.A. (Eds.), European lithosphere dynamics. Geological Society of London Memoir 32, pp. 389-405.

Okay, A.I., Sunal, G., Sherlock, S., Altıner, D., Tüysüz, O., Kylander-Clark, A.R.C., Aygül, M., 2013. Early Cretaceous sedimentation and orogeny on the active margin of Eurasia: Southern Central Pontides, Turkey. Tectonics 32, 1247-1271.

Okay, A.I., Gürsel, S., Tüysüz, O., Sherlock, S., Keskin, M., Kylander-Clark, A.R.C., 2014. Low pressure-high-temperature metamorphism during extension in a Jurassic magmatic arc, Central Pontides, Turkey. Journal of Metamorphic Geology 32, 49-69.

Okay, A.I., Altiner, D., Sunal, G., Aygül, M., Akdoğan, R., Altiner, S., Simmons, M., 2017. Geological evolution of the Central Pontides. Geological Society of London, Special Publications 464(15), SP464-3.

Ottria, G., Pandolfi, L., Catanzariti, R., Da Prato, S., Ellero, A., Frassi, C., Göncüoğlu, M.C., Marroni, M., Ruffini, L., Sayit, K., 2017. Evolution of an early Eocene pull-apart basin in Central Pontides (Northern Turkey): New insights into the origin of the North Anatolian Shear Zone. Terra Nova 29(6), 392-400.

Ozgül, N., 2012. Stratigraphy and some structural features of the Istanbul Palaeozoic. Turkish Journal of Earth Sciences 21, 817-866.

Robertson, A.H.F., 2002. Overview of the genesis and emplacement of Mesozoic ophiolites in the Eastern Mediterranean Tethyan region. Lithos 65, 1-67.

Robertson, A.H.F., Ustaömer, T., 2004. Tectonic evolution of the Intra-Pontide suture zone in the Armutlu Peninsula, NW Turkey. Tectonophysics 381, 175-209.

Robertson, A.H.F., Clift, P.D., Degnan, P.J., Jones, G., 1991. Palaeogeographical and palaeotectonic evolution of the eastern Mediterranean Neotethys. Palaeogeography, Palaeoclimatology, Palaeoecology 87, 289-343.

Şahin, Yılmaz, S., Aysal, N., Güngör, Y., Peytcheva, I., Neubauer, F., 2014. Geochemistry and U-Pb zircon geochronology of metagranites in Istranca (Strandja) Zone, NW Pontides, Turkey: implications for the geodynamic evolution of Cadomian orogeny. Gondwana Research 26, 755-771.

Sayit, K., Göncüoğlu, M.C., 2013. Geodynamic evolution of the Karakaya Mélange Complex, Turkey: a review of geological and petrological constraints. Journal of Geodynamics 65, 56-65.

Sayit, K., Marroni, M., Göncüoğlu, M.C., Pandolfi, L., Ellero, A., Ottria, G., Frassi, C., 2016. Geological setting and geochemical signatures of the mafic rocks from the Intra-Pontide Suture Zone: Implications for the geodynamic reconstruction of the Mesozoic Neotethys. International Journal of Earth Science (Geol Rundsch) 105, 39-64.

Şengör, A.M.C., Yılmaz, Y., 1981. Tethyan evolution of Turkey: a plate tectonic approach. Tectonophysics 75, 181-241.

Şengör A.M.C., Tüysüz, O., Imren, C., Sakinc, M., Eyidogan, H., Görür, N., Le Pichon, X., Rangin, C., 2005. The North Anatolian Fault: A New Look. Annual Review of Earth and Planetary Sciences 33, 37-112.

Sláma, J., Košler, J., Condon, D.J., Crowley, J.L., Gerdes, A., Hanchar, J.M., Horstwood, M.S.A., Morris, G.A., Basdala, L., Norberg, N., Schaltegger, U., Schoene, B., Tubrett, M.N., Whitehouse, M.J., 2008. Plešovice zircon - A new natural reference material for U-Pb and Hf isotopic microanalysis. Chemical Geology 249, 1-35.

Stampfli, G.M., Borel, G.D., 2002. A plate tectonic model for the Paleozoic and Mesozoic constrained by dynamic plate boundaries and restored synthetic oceanic isochrons. Earth and Planetary Science Letters 196(1), 17-33.

Stampfli, G.M., Kozur, H.W., 2006. Europe from the Variscan to the Alpine cycles. In: Gee, D.G., Stephenson, R. (Eds.), European lithosphere dynamics. Geological Society of London Memoirs 32, pp. 57-82.

Sunal, G., 2012. Devonian magmatism in the western Sakarya Zone, Karacabey region, NW Turkey. Geodinamica Acta 25, 183-201.

Sunal, G., Natal'in, B., Satır, M., Toraman, E., 2006. Paleozoic magmatic events in the Strandja Masif, NW Turkey. Geodinamica Acta 19, 283-300.

Tekin, U.K., Göncüoğlu, M.C., Pandolfi, L., Marroni, M., 2012. Middle-Late Triassic radiolarian cherts from the Arkotdağ mélange in northern Turkey: implications for the life span of the northern Neotethyan branch. Geodinamica Acta 25(3-4), 305-319.

Tokay, M., 1973. Geological observations on them North Anatolian Fault Zone between Gerede and Ilgaz. Proceedings of the North Anatolian Fault and Earthquakes Symposium, Ankara. The Mineral Research and Exploration Publication, 12-29.

Topuz, G., Altherr, R., Wolfgang, Z., Schwartz, W.H., Zack, T., Hasözbek, A., Mathias, B., Satır, M., Şen, C., 2010. Carboniferous high potassium I-type granitoid magmatism in the Eastern Pontides: the Gümüşhane pluton (NE Turkey). Lithos 116, 92-110.

Uğuz, M.F., Sevin, M., Duru, M., 2002. 1:500.000 scaled Geological map of Turkey, sheet nr.3 “SINOP”. MTA – General Directorate of Mineral Research and exploration, Ankara.

Ulianov, A., Müntener, O., Schaltegger, U., Bussy, F., 2012. The data treatment dipendent variability of U-Pb zircon ages obtained using mono-collector, sector field, laser ablation, ICPMS. Journal of Analytical Atomic Spectrometry 27(4), 663-676.

Ustaömer, P.A., Rogers, G., 1999. The Bolu Massif: remnant of a pre-Early Ordovician active margin in the West Pontides, northern Turkey. Geological Magazine 136(5), 579-592.

Ustaömer, P.A., Mundil, R., Renne, R., 2005. U/Pb and Pb/Pb zircon ages for arc-related intrusions of the Bolu Massif (W Pontides, NW Turkey): evidence for Late Precambrian (Cadomian) age. Terra Nova 17, 215-223.

Ustaömer, P.A., Ustaömer, T., Robertson, A.H.F., 2012. Ion Probe U-Pb dating of the Central Sakarya basement: a peri-Gondwana Terrane intruded by late Lower Carboniferous subduction/collision-related granitic rocks. Turkish Journal of Earth Sciences 21, 905-932.

Ustaömer, T., Robertson, A.H.F., Ustaömer, P.A., Gerdes, A., Peytcheva, I., 2013. Constraints on Variscan and Cimmerian magmatism and metamorphism in the Pontides (Yusufeli-Artvin area), NE Turkey from U-Pb dating and granite geochemistry. In: Robertson, A.H.F., Parlak, O., Ünlügenç, U.C. (Eds.), Geological development of Anatolia and the easternmost Mediterranean region. Geological Society of London, Special Publication 372, pp. 49-74.

Ustaömer, T., Ustaömer, P.A., Robertson, A.H.F., Gerdes, A., 2016. Implications of U-Pb and Lu-Hf isotopic analysis of detrital zircons for the depositional age, proveneance and tectonic setting of the Permian-Triassic Palaeotethyan Karakaya Complex, NW Turkey. International Journal of Earth Science 105(1), 7-38.

Yılmaz, Y., 1990. Allochthonous terranes in the Tethyan Middle East, Anatolia and surrounding regions. Philosophical Transaction Royal Society of London 331, 611-624.

Yılmaz, Y., Tüysüz, O., Yiğitbaş, E., Genç, C.Ş., Şengör, A.M.C., 1997. Geology and tectonic evolution of the Pontides. In: Robinson, A.G. (Eds.), Regional and petroleum geology of the Black Sea and surrounding region. American Association of Petroleum Geologists Bulletin 68, pp. 183-226.

Yılmaz, Y., Aysal, N., Güngör, Y., 2012. Petrogenesis of Late Cretaceous adakitic magmatism in the Istanbul zone (Çavuşbaşi Granodiorite, NW Turkey). Turkish Journal of Earth Sciences 21, 1029-1045.

FIGURE CAPTIONS

Fig. 1 - The major tectonic zones of Turkey separated by sutures (thick dotted lines). Neogene to Holocene active regional structures are indicated in red. The rectangle indicates the study area (modified after Frassi et al., 2018).

Fig. 2 - Geology of the study area (Modified after Catanzariti et al., 2013). a) tectonic scheme of the Daday-Arac-Bayramören area. Boxed area indicates the location of Fig.2 c. b) N-S Geological cross-section of the IPS zone. c) Close-up of the geology of the study area. The sample locations are shown by dots.

Fig. 3 - Stratigraphic features of the Taraklı Flysch in the study area. a) Reconstructed stratigraphic log of the Taraklı Flysch. The position of the studied samples are indicated on the left side of the log while the pictures position is indicated on the right. b) Lithofacies legend: 1: slide-block in shaly-matrix; 2: clast supported-conglomerates; 3: coarse-grained turbidites; 4: medium-grained arenites; 5: thin-bedded turbidites. c-g) Field occurrence of the Taraklı Flysch in the Bahcecik area. c) Thin Bedded Turbidites lithofacies; d) level of well rounded clast- to matrix-supported conglomerates (arrows) associated with coarse-grained arenites. e) well-rounded matrix-supported conglomerates showing several granitoids clasts. f) slide-blocks of Permian granitoids. g) slide-blocks of Permian granitoids (arrow) and crinoidal Devonian-Carboniferous limestones.

Fig. 4 - Field occurence and photomicrographs of the studied rocks. a) and b) quartz-monzonites (TC316). c) and d) leucocratic granodiorites (TC319). e) cm and f) mm size leucocratic granodiorite veinlets intruding quartz-monzonites. The arrows indicate the magmatic relationships.

Fig. 5 - Zircon CL images and dated spots of the samples a) TC316a, b) TC316b and c) TC319. Blue: the spots whose age has been used to calculate the weighted average age of the samples; green: the spots whose value, besides being used to calculate the weighted average age, is included within the error of the sample age. The age of the red spots has not been considered for the age calculation.

Fig. 6 - Concordia diagrams of samples TC316a and TC319 and weighted average diagrams of the samples TC316a, TC316b and TC319.

Fig. 7 - 3D reconstruction of the Taraklı Flysch depositional system and surrounding areas during the Late Cretaceous-Middle Paleocene time. The setting of the studied granitoids are indicated as a part of IZ zone as well as slide-block in the inner foredeep of the Taraklı basin.

Table 1 - Results of zircon LA-ICP-MS U-Pb age determination of the samples TC316a, TC316b, TC319. The results related to the secondary standard “Plešovice” is also reported (Sláma et al., 2008).

Figure 1
Click here to download high resolution image

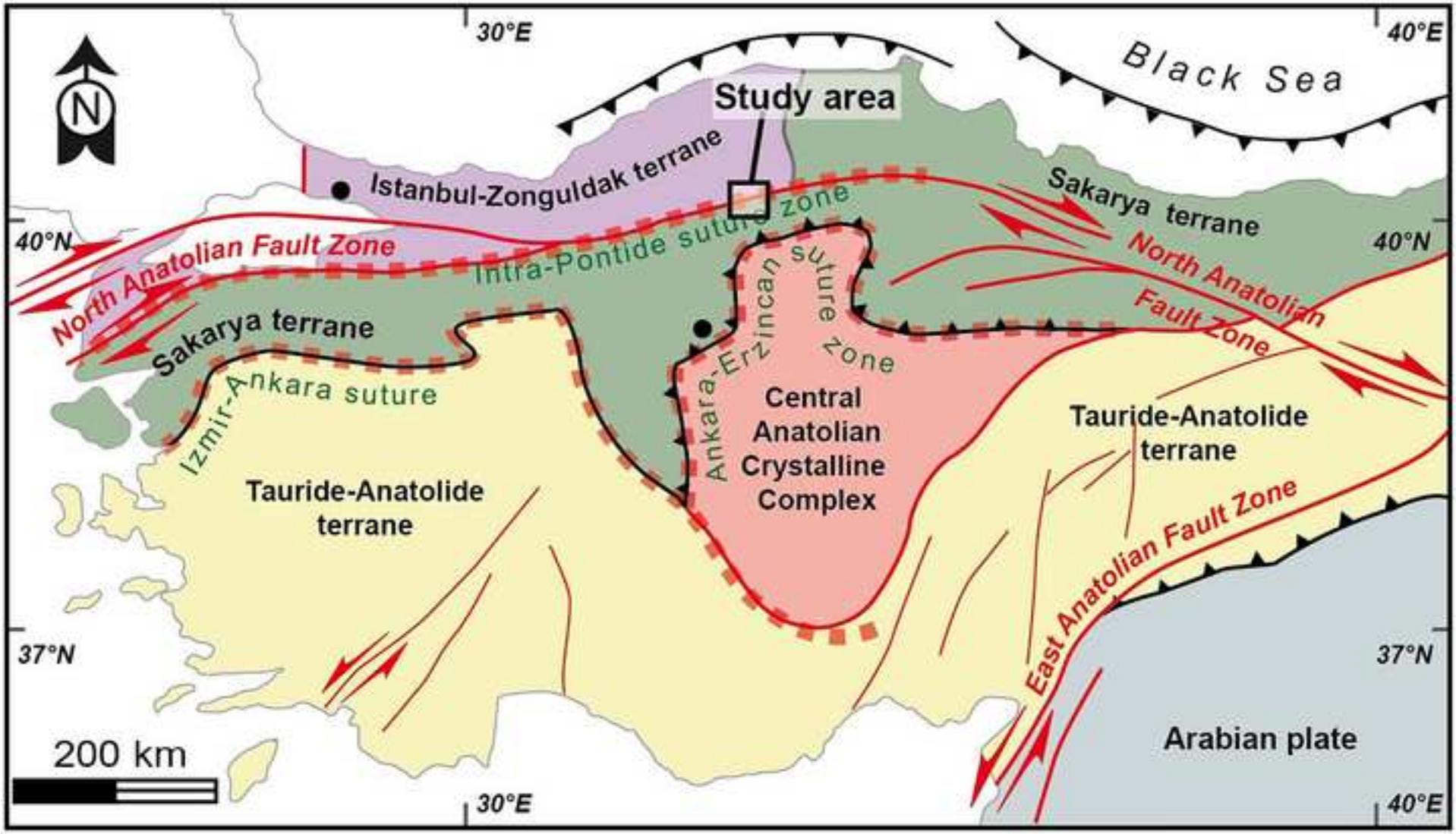

Figure 2

Click here to download high resolution image

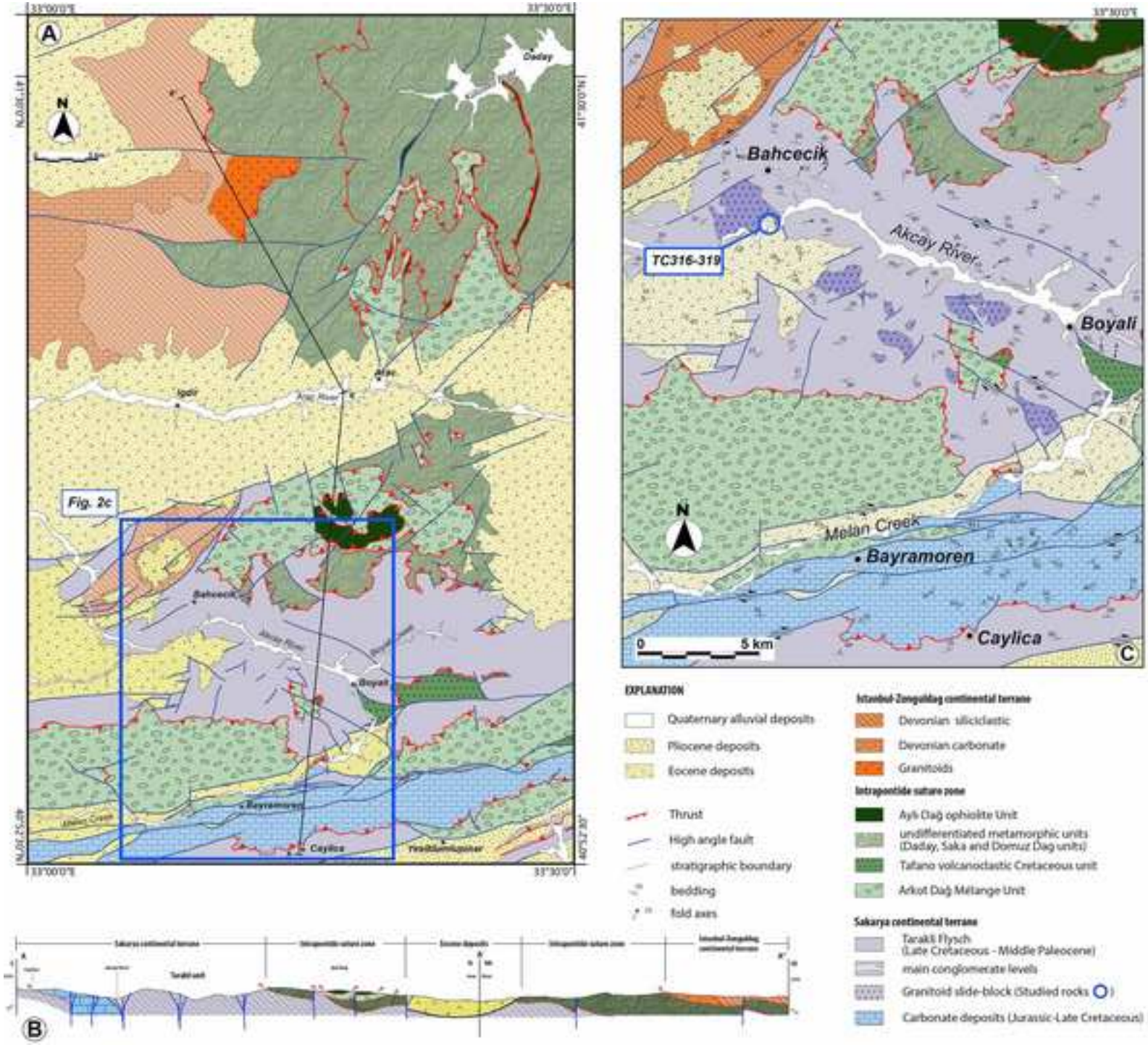

Figure 3

Click here to download high resolution image

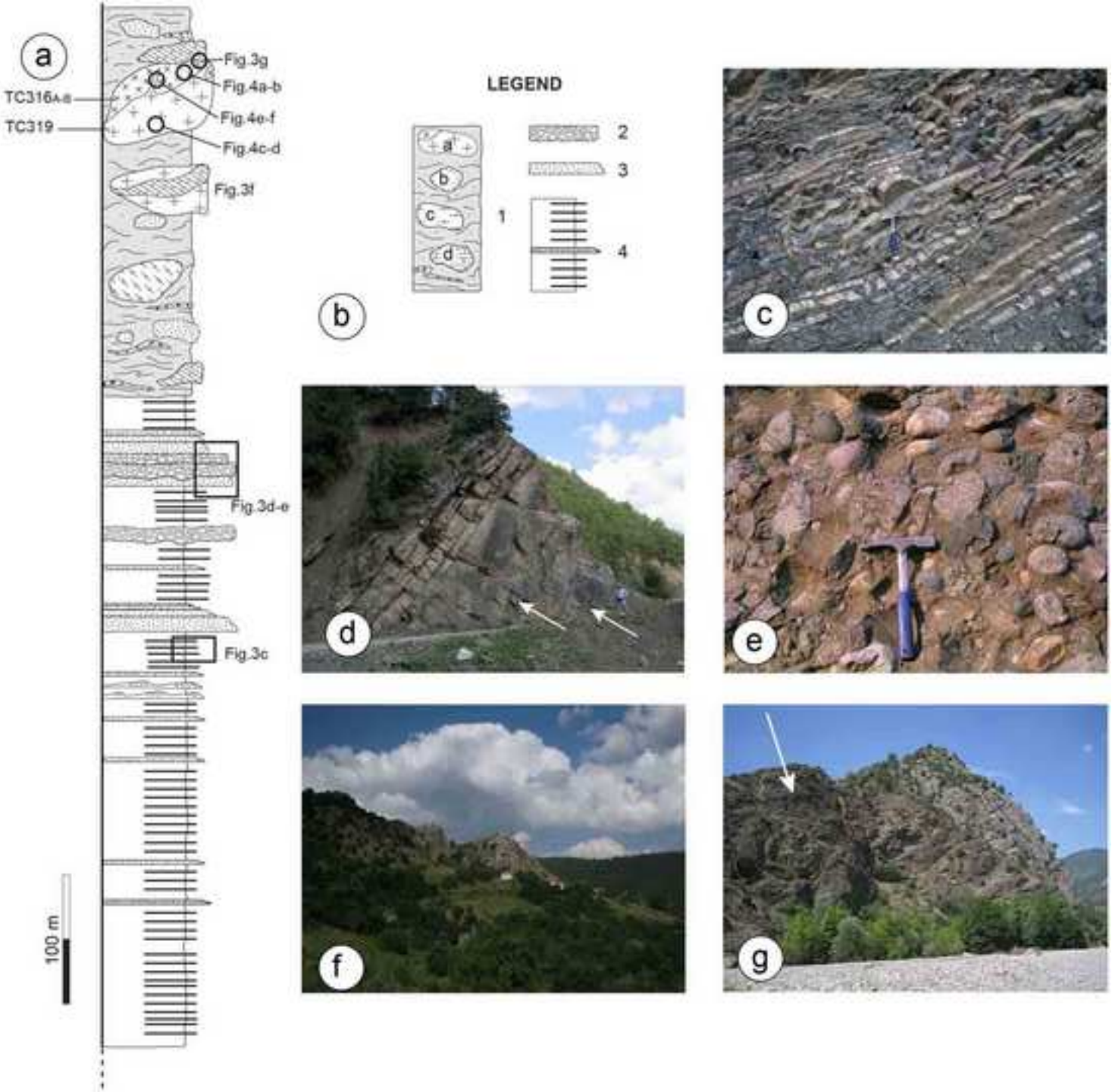

Figure 4
Click here to download high resolution image

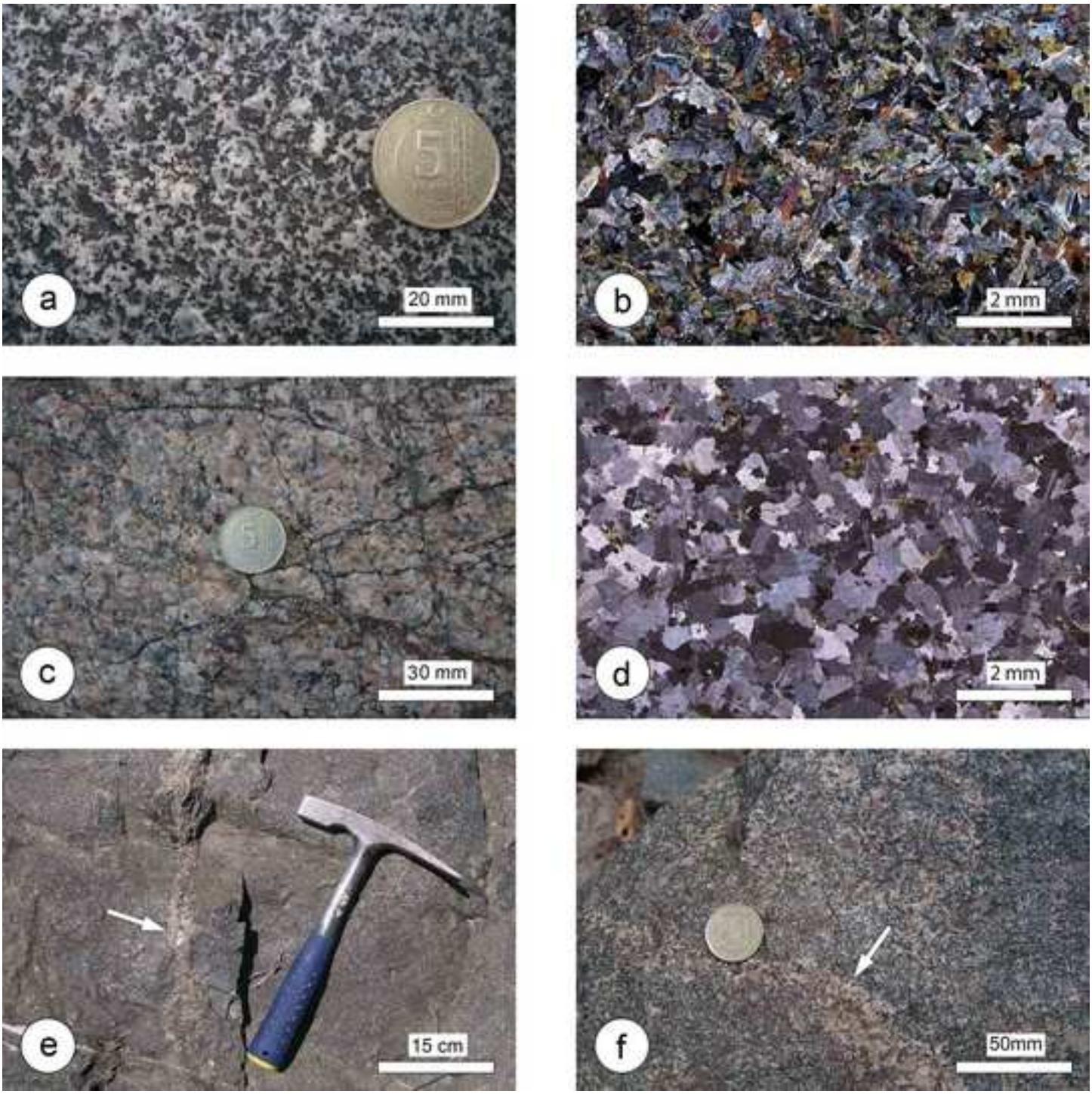

Figure 5

Click here to download high resolution image

Figure 6

Click here to download high resolution image

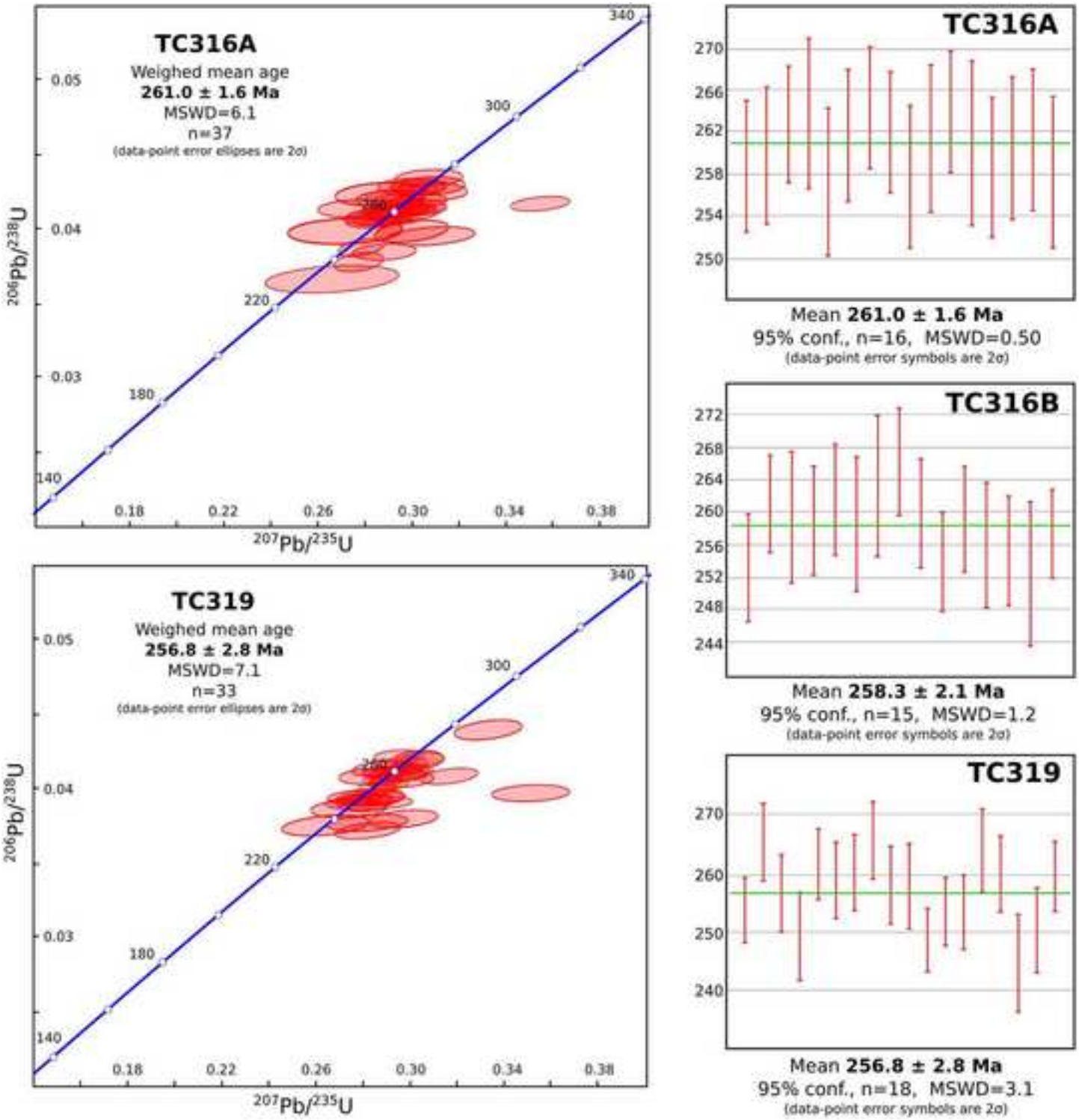

Figure 7
Click here to download high resolution image

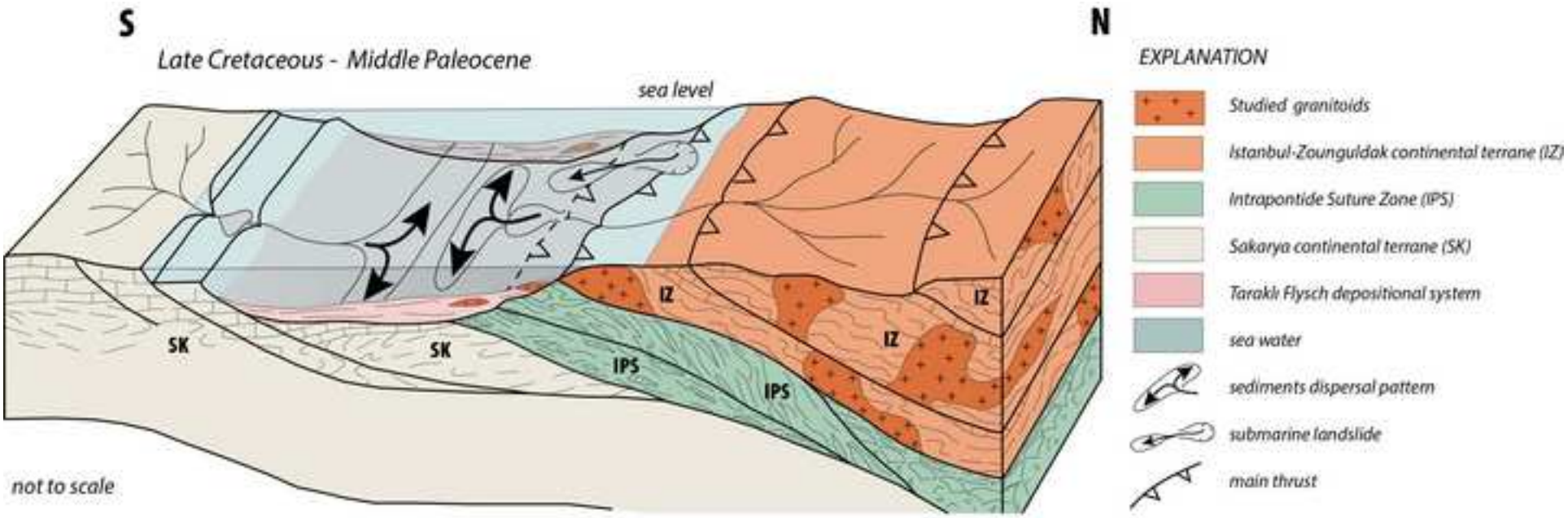

Table 1

zircon	Isotopic ratios				ρ	Age (Ma)		Apparent ages (Ma)				Conc.(%)
	$^{206}Pb/^{238}U$	2S.D.	$^{207}Pb/^{235}U$	2S.D.		$^{206}Pb/^{238}U$	S.D.	$^{207}Pb/^{235}U$	S.D.	$^{207}Pb/^{206}Pb$	S.D.	
TC316A (41°04'09.42''N, 33°09'28.86''E)												
jn11n05	0.041	0.0003936	0.2905	0.008	0.34	258.8	2.4	258.9	6.4	270	54	95.9
jn11n06	0.0411	0.00040278	0.2928	0.008	0.37	259.7	2.5	260.7	6.1	300	56	86.6
jn11n08	0.0416	0.00034112	0.2922	0.006	0.41	262.8	2.1	260.3	4.5	274	40	95.9
jn11n09	0.0399	0.00035112	0.2903	0.005	0.53	252	2.2	258.8	3.8	322	34	78.3
jn11n10	0.0418	0.00043472	0.3031	0.010	0.32	263.8	2.7	268.8	7.7	332	66	79.5
jn11n11	0.0407	0.00047212	0.2932	0.012	0.29	256.9	2.9	261.1	9.3	306	86	84.0
jn11n12	0.0378	0.00050652	0.2768	0.009	0.42	239.2	3.1	248.1	7	338	64	70.8
jn11o05	0.0418	0.00035112	0.3015	0.006	0.40	264.3	2.2	267.6	5	304	46	86.9
jn11o06	0.0428	0.00041944	0.3042	0.009	0.34	270.4	2.6	269.7	6.8	304	56	88.9
jn11o09	0.0408	0.00042432	0.2864	0.010	0.31	257.8	2.6	255.7	7.7	266	72	96.9
jn11o12	0.0388	0.0004656	0.2783	0.008	0.41	245.3	2.9	249.3	6.5	290	60	84.6
jn11o13	0.0414	0.00043884	0.3051	0.008	0.42	261.4	2.7	270.4	6	368	48	71.0
jn11o14	0.0366	0.00076128	0.2666	0.022	0.25	232	4.8	240	17.7	326	188	71.2
jn11t10	0.0418	0.00035112	0.2961	0.005	0.49	264	2.2	263.4	3.9	272	36	97.1
jn11t12	0.0413	0.00047908	0.2997	0.013	0.28	261	3	266.2	9.8	296	90	88.2
jn11v05	0.0399	0.00075012	0.2815	0.028	0.19	252.1	4.7	251.9	22.5	308	184	81.9
jn11v06	0.041	0.0004182	0.3007	0.009	0.35	258.7	2.6	266.9	6.9	338	60	76.5
jn11v07	0.0412	0.00042024	0.2964	0.009	0.34	260.5	2.6	263.6	7	306	62	85.1
jn11v08	0.0414	0.00042228	0.3041	0.008	0.37	261.3	2.6	269.6	6.5	354	56	73.8
jn11v09	0.0408	0.00045696	0.2846	0.011	0.28	258.1	2.8	254.3	9	282	86	91.5
jn11v13	0.0426	0.00039192	0.3068	0.008	0.35	269.2	2.4	271.7	6.3	290	52	92.8
TC316B (41°04'09.42''N, 33°09'28.86''E)												
jn11e05	0.04	0.00042	0.287	0.010	0.29	253.1	2.6	256.2	8	288	74	87.9
jn11e06	0.0413	0.00038	0.3006	0.008	0.34	261	2.3	266.9	6.4	332	52	78.6
jn11e08	0.0435	0.00051	0.3088	0.017	0.22	274.4	3.2	273.3	12.8	272	104	100.9
jn11e09	0.041	0.000418	0.2939	0.010	0.30	259	2.6	261.6	7.9	314	66	82.5
jn11e11	0.0414	0.00041	0.2988	0.010	0.29	261.5	2.6	265.4	8.1	276	72	94.7
jn11e12	0.0409	0.00052	0.2987	0.015	0.24	258.5	3.2	265.4	12	352	102	73.4
jn11e14	0.0422	0.00041	0.2977	0.010	0.29	266.2	2.5	264.6	7.7	262	70	101.6
jn11f05	0.0411	0.000411	0.2933	0.009	0.34	259.8	2.6	261.2	6.7	280	62	92.8
jn11f06	0.0402	0.00039	0.2815	0.009	0.30	253.9	2.4	251.8	7	264	66	96.2
jn11f07	0.041	0.000402	0.2932	0.008	0.34	259.1	2.5	261.1	6.6	294	56	88.1
jn11f09	0.0405	0.00049	0.2949	0.012	0.30	255.9	3	262.4	9.3	300	78	85.3
jn11f10	0.0404	0.00042	0.292	0.011	0.27	255.2	2.6	260.2	8.7	316	76	80.8
jn11f12	0.0407	0.00034	0.2954	0.006	0.42	257.3	2.1	262.8	4.6	308	42	83.5
jn11f13	0.04	0.00038	0.2811	0.009	0.31	253	2.3	251.5	6.8	248	60	102.0
jn11f14	0.0394	0.00039	0.274	0.007	0.37	248.9	2.4	245.9	5.7	240	56	103.7

TC319 (41°04'09.18''N, 33°09'28.98''E)												
jn11p05	0.0401	0.0003609	0.2908	0.006	0.41	253.7	2.2	259.2	5.1	338	46	75.1
jn11p06	0.042	0.0004032	0.3036	0.009	0.33	265.3	2.5	269.2	6.8	304	62	87.3
jn11p07	0.0406	0.00041412	0.2981	0.010	0.31	256.6	2.6	264.9	7.6	342	64	75.0
jn11p09	0.0394	0.00048856	0.2765	0.010	0.36	249.2	3	247.9	7.6	272	72	91.6
jn11p10	0.0414	0.00036432	0.2951	0.007	0.35	261.6	2.3	262.5	5.8	292	54	89.6
jn11p12	0.041	0.00041	0.2964	0.008	0.38	258.8	2.5	263.6	6.1	306	56	84.6
jn11p13	0.0439	0.0005268	0.3333	0.011	0.35	277	3.2	292.1	8.7	420	70	66.0
jn11q05	0.0412	0.00040376	0.2866	0.009	0.30	260.1	2.5	255.9	7.4	298	58	87.3
jn11q06	0.0421	0.00040416	0.295	0.009	0.32	265.6	2.5	262.5	7	258	60	102.9
jn11q14	0.039	0.0004524	0.2822	0.015	0.22	246.3	2.8	252.4	11.9	352	104	70.0
jn11t05	0.0408	0.0004488	0.2952	0.010	0.31	257.8	2.8	262.7	8.2	290	70	88.9
jn11t06	0.0393	0.00036156	0.2883	0.008	0.32	248.6	2.2	257.3	6.5	326	58	76.3
jn11z05	0.0377	0.00055796	0.2813	0.014	0.29	238.3	3.4	251.7	11.5	352	110	67.7
jn11z06	0.0401	0.00036892	0.287	0.008	0.35	253.4	2.3	256.2	6	286	60	88.6
jn11z07	0.0401	0.00039298	0.2873	0.009	0.30	253.3	2.5	256.5	7.3	300	70	84.4
jn11z08	0.0418	0.00043472	0.3048	0.008	0.40	264	2.7	270.1	6.2	320	54	82.5
jn11z09	0.0411	0.00039456	0.2907	0.009	0.30	259.9	2.5	259.1	7.2	260	64	100.0
jn11z10	0.0387	0.0005418	0.2737	0.013	0.29	244.7	3.4	245.6	10.5	294	102	83.2
jn11z11	0.0375	0.0006	0.2647	0.016	0.27	237.5	3.7	238.5	12.8	264	130	90.0
jn11z12	0.0396	0.00045936	0.2819	0.011	0.29	250.2	2.9	252.2	8.8	242	84	103.4
jn11z13	0.0411	0.00037812	0.2988	0.009	0.32	259.5	2.3	265.5	6.7	332	58	78.2
Plešovice												
ples-a15	0.0535	0.000417	0.4025	0.008	0.39	335.9	2.6	343.5	5.8	392	40	85.7
ples-b15	0.054	0.000421	0.3954	0.008	0.39	338.8	2.6	338.3	5.8	330	40	102.7
ples-b16	0.0538	0.000463	0.3957	0.009	0.38	337.8	2.8	338.5	6.5	334	46	101.1
ples-c15	0.054	0.000432	0.4008	0.007	0.43	339	2.7	342.2	5.4	356	38	95.2
ples-d15	0.0536	0.000429	0.4008	0.010	0.33	336.9	2.6	342.2	7.1	372	50	90.6
ples-e16	0.0536	0.00045024	0.4031	0.009	0.36	336.3	2.7	343.9	6.8	378	44	89.0
ples-f16	0.0538	0.0004842	0.3915	0.009	0.40	337.9	2.9	335.4	6.5	322	46	104.9
ples-h15	0.054	0.000454	0.3924	0.009	0.35	339.1	2.8	336.1	6.9	318	50	106.6
ples-i15	0.0537	0.000462	0.4098	0.010	0.37	337.1	2.8	348.8	6.9	402	44	83.9
ples-i16	0.0537	0.000473	0.3991	0.011	0.33	337.4	2.9	341	7.6	348	50	97.0
ples-m15	0.0536	0.000461	0.3847	0.007	0.45	336.9	2.8	330.5	5.4	312	40	108.0
ples-m16	0.0539	0.000464	0.4001	0.008	0.41	338.7	2.8	341.7	6.1	356	42	95.1
ples-n16	0.0537	0.00047256	0.4011	0.008	0.43	337.3	2.9	342.5	5.9	382	38	88.3
ples-o16	0.0538	0.00045192	0.3964	0.008	0.42	337.6	2.8	339	5.8	348	44	97.0
ples-p15	0.0539	0.00044198	0.3952	0.008	0.41	338.2	2.7	338.2	5.7	344	38	98.3
ples-r15	0.054	0.000475	0.4062	0.009	0.42	339.1	2.9	346.2	6.2	354	38	95.8
ples-t15	0.0535	0.0004387	0.3993	0.008	0.39	336.1	2.7	341.1	6.1	378	40	88.9
ples-t16	0.054	0.000486	0.3937	0.010	0.37	338.9	2.9	337.1	7	338	50	100.3
ples-u16	0.0537	0.000451	0.3946	0.008	0.42	336.9	2.7	337.7	5.7	350	42	96.3
ples-v15	0.0535	0.0004815	0.3905	0.008	0.42	336	3	334.7	6.1	338	42	99.4
ples-z16	0.0535	0.0004922	0.404	0.009	0.42	335.8	3	344.5	6.4	386	40	87.0

Graphical Abstract (for review)